Photoinitiated decomposition of HNCO near the H+NCO threshold: Centrifugal barriers and channel competition

M. Zyrianov, A. Sanov,[a] Th. Droz-Georget,[b] and H. Reisler[c]
Department of Chemistry, University of Southern California, Los Angeles, California 90089-0482

(Received 8 January 1999; accepted 16 March 1999)

The decomposition of jet-cooled HNCO is investigated near the H+NCO channel threshold [D_0(H+NCO)=38 370 cm^{-1}]. Dissociation to H+NCO at energies 17–411 cm^{-1} above D_0(H+NCO) proceeds on the ground potential energy surface (S_0), apparently without a barrier. The rotational state distributions of the NCO($X\,^2\Pi_{3/2}$,00^{1}0) fragment are well described by phase space theory (PST), provided that dynamical constraints are included. These constraints are associated with long range (4–7 Å) centrifugal barriers, which are significant even near threshold because of the small reduced mass of H+NCO, and result in a fraction of energy deposited in fragment rotation much smaller than predicted by unconstrained PST. The influence of orientation averaging on the attractive, long-range part of the potential is discussed, and it is argued that angular averaging with respect to the center of mass of the rotating polyatomic fragment results in a shift in the effective potential origin, accompanied by an attenuation of the magnitude of the potential compared to its value for fixed H–N distance. Following initial $S_1(^1A'')\leftarrow S_0(^1A')$ excitation and internal conversion to S_0, HNCO(S_0) decays both via unimolecular decomposition of H+NCO and intersystem crossing to the dissociative first triplet state, T_1 [yielding NH($X\,^3\Sigma^-$)+CO products]. The competition between the two processes is interrogated by monitoring changes in the relative yields of NCO and NH($X\,^3\Sigma^-$) as a function of excitation energy. It is concluded that near D_0(H+NCO), the $S_0\rightarrow T_1$ intersystem crossing rate is several-fold faster than the H+NCO unimolecular decomposition rate. © *1999 American Institute of Physics.*
[S0021-9606(99)00722-9]

I. INTRODUCTION

Studies of photoinitiated unimolecular reactions have contributed greatly to our understanding of chemical change at the most fundamental level. Examinations of the near-threshold region have been particularly revealing in identifying barriers, symmetry and angular momentum constraints, the nature of the transition state (TS), fluctuations, and quantum interference effects.[1–6] In addition, the importance of weak mixings among zero-order states, incomplete intramolecular vibrational redistribution (IVR), the ''goodness'' of selected quantum numbers, and changes in the density of states have been critically examined in the threshold region.[6–8] In molecules with large density of states, IVR is usually complete, and state-to-state fluctuations and quantum interference effects naturally average out. In such cases, treatments of the dissociation using TS theories to calculate the average rates and product state distributions have proven quite successful,[1–6] even at the level of correlated product distributions.[9,10]

In a rate description, the average transition rate, $k(E)$, from a discrete state to a continuum (or quasicontinuum) can be described using Fermi's Golden Rule:

$$k(E)=\langle\Gamma(E)\rangle/\hbar=2\pi\langle v\rangle^2\rho_f(E)/\hbar, \tag{1}$$

where $\langle\Gamma(E)\rangle$ is the average decay width, $\langle v\rangle$ is the average coupling matrix element, and $\rho_f(E)$ is the final-state density of states. The average rate of a unimolecular reaction evolving via vibrational predissociation is given by TS theory as:

$$k(E)=N^\dagger(E)/h\rho(E), \tag{2}$$

where $N^\dagger(E)$ is the number of open channels in the TS, and $\rho(E)$ is the density of states of the excited complex.

In this paper, we examine the threshold region of the unimolecular decomposition of jet-cooled HNCO on the ground state (S_0), as well as the competition between decomposition to H+NCO and intersystem crossing (ISC) to the lowest triplet state (T_1). The absence of fluctuations in the product state distributions, the simplicity of modeling an atom+linear fragment dissociation by statistical theories, and the large number of NCO rotational levels populated even at low excess energies make this system attractive for examination of dynamical constraints in the exit channel of barrierless dissociation.

The photoinitiated unimolecular decomposition of HNCO following $S_1(^1A'')\leftarrow S_0(^1A')$ optical excitation leads to three product channels:

$$\mathrm{NH}(X\,^3\Sigma^-)+\mathrm{CO}(X\,^1\Sigma^+)\quad \Delta H=30\,060\pm30\ \mathrm{cm}^{-1}, \tag{I}$$

$$\mathrm{H}(^2S)+\mathrm{NCO}(X\,^2\Pi)\quad \Delta H=38\,370\pm30\ \mathrm{cm}^{-1}, \tag{II}$$

$$\mathrm{NH}(a\,^1\Delta)+\mathrm{CO}(X\,^1\Sigma^+)\quad \Delta H=42\,750\pm25\ \mathrm{cm}^{-1}. \tag{III}$$

[a]Present address: JILA, National Institute of Standards and Technology and University of Colorado, Boulder, CO 80309-0440.
[b]Present address: Novartis Services AG, K-127.6.78 CH-4002 Basel, Switzerland.
[c]Author to whom correspondence should be addressed; e-mail: reisler@chem1.usc.edu

In what follows, NH($X\,^3\Sigma^-$) and NH($a\,^1\Delta$) are denoted by ^{3}NH and ^{1}NH, respectively. Dissociation to channel II has received considerable attention.[11–22] Earlier studies at high photolysis energy (193 nm) concluded that products accrue via direct dissociation on the excited $S_1(\,^1A'')$ state potential energy surface (PES).[13] The quantum yield for this channel was measured over a broad excitation energy range,[11,16] and the possibility to affect the yield (relative to the yield of channels I and III) by implanting vibrational excitation in the molecule prior to the photolysis step was demonstrated.[18] It was also established that near its threshold, channel II dissociation proceeded not directly on S_1, but rather via internal conversion (IC) to S_0 followed by unimolecular decomposition on S_0, apparently without a barrier.[18–22] The barrier on S_1 to channel II dissociation was found by both experiment and theory to be at least 8000 cm^{-1} above D_0(H+NCO).[20–22] Linewidths near D_0(H+NCO) are of the order of a wave number, corresponding to an IC time scale of few picoseconds.[14,15] Fragment angular anisotropy measurements indicate that the appearance times of H+NCO exceed 10 ps.[16,19,20]

Recently, we proposed that the pathway to channel I following S_1 excitation is $S_1 \rightarrow S_0 \rightarrow T_1$, at least up to the opening of channel III.[20] Thus above D_0(H+NCO), HNCO(S_0) can decay via two competing pathways, one involving ISC to the dissociative T_1 surface, and the other—coupling to the channel II dissociative continuum on S_0. Here, we present evidence that near the channel II threshold, the rate of formation of ^{3}NH+CO is several-fold faster than the rate of formation of H+NCO. We also compare the rotational state distributions of NCO($^2\Pi_{3/2}$) products at available energies $E_{avl}=17-411\,cm^{-1}$ above D_0(H+NCO) to the predictions of phase space theory (PST).[23,24] Stringent angular momentum constraints due to centrifugal barriers in the long-range part of the ground-state PES are revealed. Owing to the small reduced mass of H+NCO ($\mu \approx 1$ a.m.u.) and the small rotational constant of NCO ($B_{NCO}=0.39\,cm^{-1}$),[25] these constraints are clearly manifest even in the vicinity of the threshold.

II. EXPERIMENT

The experimental arrangement used in the laser-induced fluorescence (LIF) pump–probe experiments employed here was described previously.[14,26] Isocyanic acid (HNCO) is prepared and purified following published procedures,[27] and seeded in a 30:70 He:Ne mixture at a typical pressure of 760 Torr. The expansion-cooled HNCO has a rotational temperature $T_{rot} \approx 10$ K. The counterpropagating pump and probe laser beams are collimated to ~2 mm diameter, and intersect the jet at ~5 mm distance from the 0.5 mm nozzle orifice. The delay between the pump and probe lasers pulses is set at 50 ns. HNCO is photolyzed near the channel II threshold (~260 nm) with typical pulse energies of 1–2 mJ using the unfocused output of an excimer laser pumped dye laser.

The NCO($X\,^2\Pi_{3/2}$) products are probed by laser-induced fluorescence (LIF) via the $A\,^2\Sigma^+ \leftarrow X\,^2\Pi$ transition,[25] using a second excimer laser pumped dye laser at 50 ns pump–probe delay. To minimize saturation effects, the probe laser pulse energy is kept at <5 μJ. Still, the most intense features of the NCO LIF spectra (the *Q*-branch bandheads) may be slightly affected by saturation. Fluorescence is collected with *f*/1.5 optics and detected by a photomultiplier tube in the 400–500 nm range using appropriate glass filters.[28] The ^{3}NH products are detected via the $A\,^3\Pi \leftarrow X\,^3\Sigma^-$ transition using the frequency-doubled output of a Nd:YAG laser pumped dye laser, as described previously.[29]

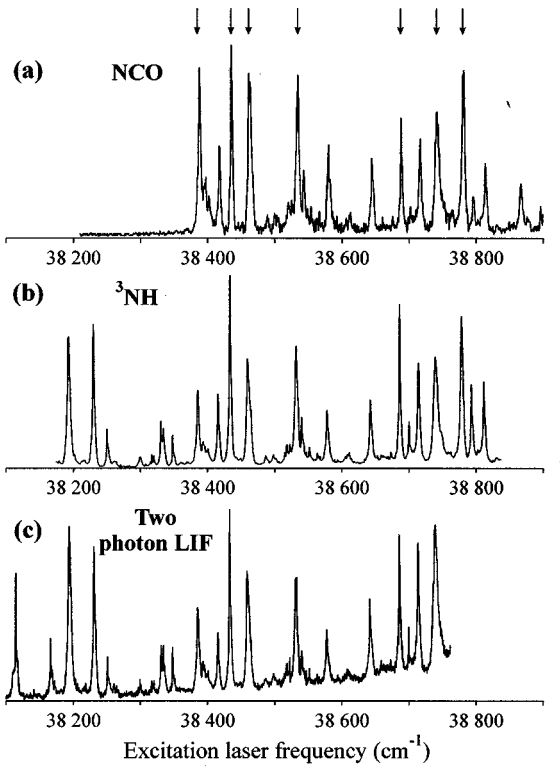

FIG. 1. (a) The NCO photofragment yield spectrum obtained in the photodissociation of HNCO by monitoring the Q_{11} bandhead (low *J*) of the $(00^00-00^10)A\,^2\Sigma^+ \leftarrow X\,^2\Pi$ transition. Arrows mark the peaks where complete LIF spectra of the NCO fragment are obtained. (b) The ^{3}NH yield spectrum obtained in the photodissociation of HNCO by monitoring the Q_1 branch of the $A\,^3\Pi \leftarrow X\,^3\Sigma^-$ transition. (c) Two-photon excitation spectrum of jet-cooled HNCO near D_0(H+NCO) obtained via the $S_1 \leftarrow S_0$ transition by monitoring NCO($A \rightarrow X$) fluorescence as described in Ref. 14.

III. RESULTS AND ANALYSIS

Figure 1 presents the NCO photofragment yield spectrum near D_0(H+NCO), and compares it to spectra obtained previously by monitoring the ^{3}NH fragment and the HNCO fluorescence induced by two-photon excitation.[14,29] The latter is proportional to the HNCO absorption spectrum. The ^{3}NH yield spectra were obtained by monitoring the $A\,^3\Pi \leftarrow X\,^3\Sigma^-$ Q_1 bandhead (the largest peaks in the ^{3}NH fragment LIF spectra) corresponding to rotational levels $N>6$. In the NCO yield spectra, the Q_{11} bandhead of the NCO $A\,^2\Sigma^+ \leftarrow X\,^2\Pi_{3/2}(00^00-00^10)$ transition (low *J*'s) was monitored.[25] Vertical arrows indicate excitation energies at which NCO photofragment LIF spectra were obtained. Transitions originating from the second spin-orbit state of NCO (i.e., the $^2\Pi_{1/2}$ state, which lies 94.8 cm^{-1} above the ground $^2\Pi_{3/2}$ state) were not monitored.

Yield spectra of NCO were also obtained by monitoring the (030) $\mu\,^2\Sigma^+$, (030) $\mu\,^2\Delta$, and $(100)^2\Pi_{3/2}$ vibrational

states of NCO near their respective thresholds.[25] The LIF signals associated with both the bending and the stretching vibrational levels appeared at their respective energetic thresholds exhibiting no noticeable constraints, contrary to the conclusion of previous work.[15] However, hot-band excitation in the previous 300 K experiments might have affected the measured NCO distributions, and an incorrect value for the channel II threshold was used in the analysis.

The LIF spectra of NCO($^2\Pi_{3/2}$,00^10) fragments at specific excitation energies were compared to stimulated spectra, in which the rotational level populations were calculated by PST.[23,24] The simulations were carried out as follows. First, the rotational level energies in the $A\,^2\Sigma^+$ and $X\,^2\Pi_{3/2}$ states and the corresponding spectral line positions were calculated.[25] Second, PST was used to obtain the rotational level populations,[2,23,24] taking into account the parent HNCO angular momentum, J_{HNCO}, and the rotational excitation energy resulting from the finite temperature in the molecular beam (10 K). Third, the level populations were multiplied by the corresponding rotational line-strength factors to yield line intensities.[25] Finally, the calculated spectral lines were convoluted with the Gaussian laser line shape of 0.25 cm^{-1} width.

Since the measured NCO rotational excitations were lower than predicted by unconstrained PST (see below), we applied two methods to constrain the model distributions. In the first approach, we used a single fit parameter, $b_{\max}$, representing the largest allowed impact parameter for the separating H and NCO fragments. In the second approach, we employed the centrifugal barrier restriction to describe the constraint.

The impact parameter b is related to the orbital angular momentum quantum number L of the separating products by:

$$(\mu v b)^2=\hbar^2 L(L+1), \tag{3}$$

where v is the relative velocity of the separating products. In the constrained PST calculations, we did not count phase space ($J\times L$) cells with a quantum number L corresponding to an impact parameter b in excess of $b_{\max}$.

Shown in Fig. 2(a) is the NCO LIF spectrum recorded at photolysis energy 411 cm^{-1} above the channel II threshold. The triangles on top of the measured peaks represent the calculated peak intensities in the simulated spectrum obtained using $b_{\max}=4$ Å. Figure 2(b) presents a simulated spectrum for the same E_{avl}, but with no impact parameter constraint ($b_{\max}=50$ Å). Clearly, the impact parameter restriction is essential for achieving a satisfactory fit.

Figure 2(c) displays the NCO fragment LIF spectrum recorded with the photolysis laser parked at the first peak in the yield spectrum in Fig. 1, which corresponds to $E_{\mathrm{avl}}=17\,\mathrm{cm}^{-1}$. Again, the filled triangles represent the peak intensities in the simulated spectrum; however, the best fit is achieved with $b_{\max}=7$ Å. The other spectra obtained at the photolysis energies indicated by arrows in Fig. 1(a) are best modeled by using $b_{\max}$ values which progressively decrease from 7 ± 1 Å for $E_{\mathrm{avl}}=17\,\mathrm{cm}^{-1}$ to 4 ± 0.5 Å for $E_{\mathrm{avl}}=411\,\mathrm{cm}^{-1}$.[28]

Since the available energy for the spectrum shown in Fig. 2(c) is within the error bars reported for D_0(H+NCO),

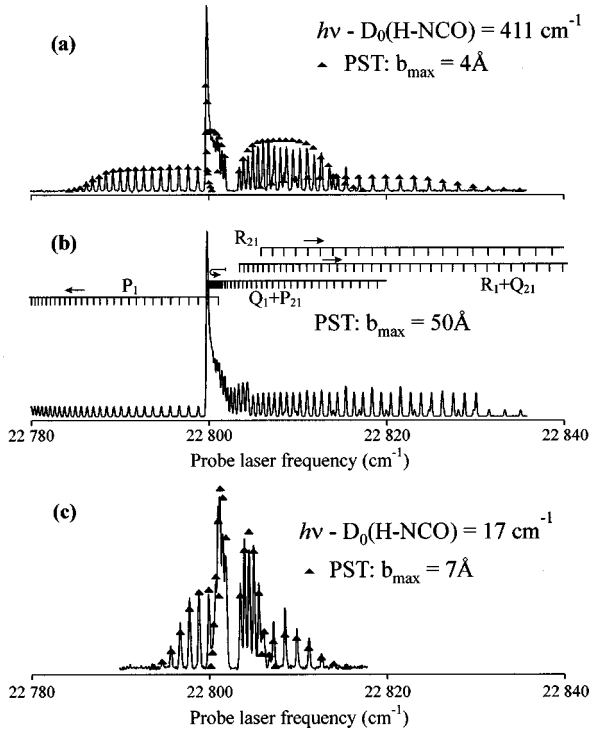

FIG. 2. (a) The solid lines are the experimental LIF spectrum of NCO($^2\Pi_{3/2}$;00^10) obtained via the (00^00-00^10) $A\,^2\Sigma^+\leftarrow X\,^2\Pi$ transition at $E_{\mathrm{avl}}=411\,\mathrm{cm}^{-1}$. The triangles mark the corresponding peak heights for a simulated spectrum in which the rotational populations are calculated with PST using the impact-parameter constraint with $b_{\max}=4$ Å. (b) Simulated spectrum of NCO at the same E_{avl}, obtained using unconstrained PST to calculate the rotational distributions. (c) The solid lines are the experimental LIF spectrum of NCO($^2\Pi_{3/2}$;00^10) obtained at $E_{\mathrm{avl}}=17\,\mathrm{cm}^{-1}$. The triangles are the corresponding peak heights in a simulated spectrum in which the rotational populations are calculated by PST using $b_{\max}=7$ Å.

a question arises regarding the accuracy of this value and its influence on the derived fit. We find that adequate modeling of all the NCO(00^10) LIF spectra in the range $E_{\mathrm{avl}}=17-411\,\mathrm{cm}^{-1}$ can be achieved by using a single value of $b_{\max}=4$ Å, *provided the D_0(H+NCO) threshold energy is lowered by 20 cm^{-1}*. However, the appearance thresholds and rotational distributions of the other monitored vibrational levels near their respective thresholds cannot be modeled well when D_0(H+NCO) is reduced by more than 7 cm^{-1}. Note also that D_0(H+NCO) was derived from the spectrum in Fig. 1(a), and the quoted error bars include the uncertainty in the *absolute* laser wavelength calibration. On the other hand, E_{avl} is a *relative* quantity determined over a relatively narrow wavelength region, and therefore its accuracy is much higher than the accuracy of D_0. Pursuant to the above, $D_0(\mathrm{H+NCO})=38\,370\,\mathrm{cm}^{-1}$ was used in the present modeling.

The second approach to restricting the rotational state distributions is based on the centrifugal barrier constraint.[1,2] In this model, the effective potential for interaction of the separating H and NCO fragments is assumed to be given by:

$$V_{\mathrm{eff}}=V(r)+V_L(R)=-\frac{C_6}{r^6}+\frac{\hbar^2 L(L+1)}{2\mu R^2}, \tag{4}$$

where the first (attractive) part $V(r)$ is defined by the long-

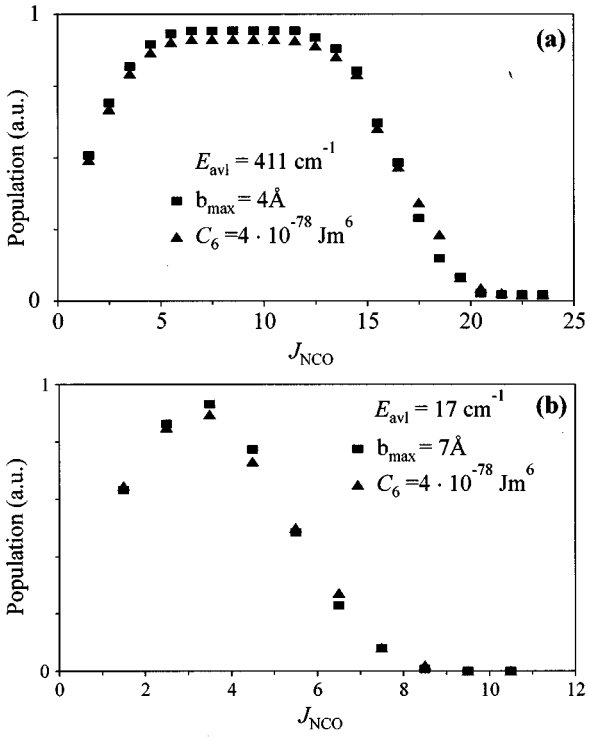

FIG. 3. The NCO($^2\Pi_{3/2}$) rotational populations that best fit the experimental LIF spectra shown in Fig. 2. The populations are calculated by PST using an impact-parameter (b_{max}) constraint (squares) and a centrifugal-barrier constraint [Eq. (4)] with $C_6=4\times10^{-78}$ J m^6 (triangles) at parent HNCO rotational temperature, $T_{rot}=10$ K. The available energies are (a) $E_{avl}=411$ cm^{-1}, and (b) $E_{avl}=17$ cm^{-1}.

range part of the Lennard-Jones (LJ) potential describing the S_0 PES along the H-NCO reaction coordinate, while the centrifugal ''force'' is responsible for the repulsion term $V_L(R)$. Note that the two terms depend on different coordinates: in $V(r)$, r is usually associated with the length of the breaking chemical bond, while in $V_L(R)$, R is the distance between the centers of mass of the products. Equating r and R is correct only for diatomic dissociation, while in polyatomics, the position and height of the centrifugal barrier depend on the relative orientation of the fragments, complicating the PST state count. Here, we assume diatomiclike dissociation and use Eq. (4) with $r=R$; this approximation is further scrutinized in Sec. IV and in the Appendix.

In the PST calculations, phase space cells for which the centrifugal barrier height exceeds the available translational energy of the fragments are not counted, and the C_6 coefficient in Eq. (4) is the only fit parameter. We find that all the experimental spectra in the range $E_{avl}=17-411$ cm^{-1} can be well fit using $C_6=(4\pm2)\times10^{-78}$ J m^6. Figure 3 presents a comparison between the two restricting models that fit the experimental spectra displayed in Fig. 2; clearly, the differences are insignificant.

IV. DISCUSSION

A. NCO product state distributions

1. Dynamical barriers

The good fit of the NCO rotational distributions to the constrained PST model indicates that the unimolecular decomposition of HNCO takes place on a barrierless PES and evolves via a fairly loose TS. Since $S_0\rightarrow T_1$ ISC constitutes an additional decay route, time-resolved measurements alone cannot provide a good test of statistical decomposition, and the knowledge of product state distributions is crucial for revealing the nature of the TS. The >10 ps time scale, inferred for decay on S_0,[20] is sufficiently long for complete IVR in the parent. The rotational distributions are subject to severe dynamical constraints even though the PES is barrierless. This is not surprising, since the orbital angular momentum constraint is stringent in reactions involving hydrogen bond fission (small reduced mass). The constraint can be characterized either by a b_{max} parameter, or by a parameter associated with a centrifugal barrier, with both approaches reflecting the same dynamics.

For HNCO→H+NCO, angular momentum conservation requires that

$$\mathbf{J}_{HNCO}=\mathbf{J}_{NCO}+\mathbf{L}+\mathbf{S}_H, \tag{5}$$

where $\mathbf{J}_{HNCO}$ and $\mathbf{J}_{NCO}$ are the total angular momentum vectors of the parent HNCO and the NCO fragment, respectively, and $\mathbf{S}_H$ is the electron spin of the atomic hydrogen fragment. Since both J_{HNCO} and S_H are small, $\mathbf{J}_{NCO}$ must be predominantly counterbalanced by the orbital angular momentum $\mathbf{L}$ of the recoiling fragments. Close to D_0(H+NCO), the highest energetically accessible J_{NCO} increases rapidly with E_{avl}. For example, for 10 K HNCO only rotational levels up to $J_{HNCO}=6-7$ are significantly populated, while at $E_{avl}=200$ cm^{-1}, the highest energetically accessible J_{NCO} is 22.5. Thus large values of $L(L\sim J_{NCO})$ are required by Eq. (5) for the formation of NCO in rotational levels close to the energetic maximum. On the other hand, high J_{NCO} levels are correlated energetically with small translational energies (small v), and therefore the associated large L values can mandate unphysically large values of the impact parameter b. One way of eliminating such unphysical phase-space cells from the PST state count is to employ a dynamical b_{max} restriction, as described in Sec. III. The simulated NCO LIF spectrum shown in Fig. 2(a) was obtained with $b_{max}=4$ Å, a distance characteristic of a van der Waals-type interaction rather than chemical bonding. This is also a typical location of a loose PST-like TS. Notice that the constraint limits J_{NCO} to $\leqslant20.5$, substantially below the maximum value $J_{NCO}=34.5$ allowed by the energetics.

To achieve a good fit closer to D_0(H+NCO), b_{max} must be increased up to 7 Å. Assuming that the TS is located near the top of the dynamical barrier, the increase in b_{max} is associated with the loosening of the TS as the threshold is approached, which is a general characteristic of barrierless unimolecular reactions.[1,2] The large b_{max} values obtained here for values of $E_{avl}<400$ cm^{-1} suggest that the dynamical barriers can be attributed to the centrifugal ''force'' in Eq. (4), and therefore their heights and locations should depend on L.

Several approximations and assumptions are made in the PST calculations that include the centrifugal barrier constraint: (i) the H-NCO potential is taken to be isotropic with respect to the relative orientation of the fragments, and $r=R$ is assumed in Eq. (4) (diatomiclike dissociation); (ii) the

long-range attractive part of the potential is described by a single term $-C_6/R^6$, where R is the distance between the centers of mass of the fragments; and (iii) no interaction between the fragments is assumed beyond the TS, which is placed at the top of the centrifugal barrier, i.e., a channel is considered closed if the product c.m. translational energy is smaller than the height of the centrifugal barrier for the corresponding L.

Assumption (i) needs to be reconciled with the anisotropy of fragment interactions. One approach, particularly suitable for barrierless dissociation, involves transforming the isotropic potential $V(r)$ into the angle-dependent potential $V(R,\theta)$ followed by averaging with respect to the orientation angle θ. Since an underlying assumption of PST is that the entire phase space is sampled when the TS is loose, orientation averaging is a sensible approach. In the Appendix, we suggest a simple expression for the orientation-averaged $1/r^6$ potential. For HCNO, the existence of several bound structural isomers (e.g., HOCN, HCNO) with equilibrium energies below D_0(H+NCO) should make the interaction potential appear more isotropic on average.

Despite the apparent crudeness of the pseudo-diatomic approximation, we are able to model all the NCO LIF spectra at $E_{\rm avl}=17-411\,{\rm cm}^{-1}$ by using $C_6=(4\pm2)\times10^{-78}\,{\rm J\,m}^6$. This value is comparable to $C_6=1.76\times10^{-78}\,{\rm J\,m}^6$ obtained for hydrogen fission from ethylene,[2] and to $C_6\approx3\times10^{-78}\,{\rm J\,m}^6$ that best fits the distributions of the hydrogen channel in the S_0 dissociation of formaldehyde.[30]

It is uncertain to what extent the success of the single-parameter fits results from the validity of the assumptions. As discussed in the Appendix, a pseudo-diatomic form of $V(r)$ can describe rather well the long-range part of the potential, while failing at shorter distances. Since it is the long-range potential that is most important for a loose, PST-like TS, the success of the pseudo-diatomic approximation may be a reflection of the mere geometrical fact that at long range $r\approx R$. The value of the C_6 coefficient given by using the approximate treatment [Eq. (4) with $r=R$] is about a factor of 2 larger than what would be obtained with an angle-averaged potential (see Appendix). Also, we recognize that the simple r^{-6} dependence used to model the H+NCO interaction is an oversimplification. For example, in other radical–radical systems the long-range part of the PES is often more attractive than described by the LJ potential.[1,2] Nevertheless, it is clear that a centrifugal-barrier constraint in PST is essential for a correct description of the NCO rotational distributions.

It is not surprising that the $b_{\rm max}$ parameter and centrifugal-barrier approaches lead to similar fragment rotational distributions, because both models reflect the same physical reality. In both cases, phase space is restricted to exclude interactions between the fragments beyond a limiting separation. In the $b_{\rm max}$ approach, the cutoff distance is used as an arbitrary fitting parameter. The centrifugal-barrier approach lends a dynamical interpretation to the limiting separation r_0, which is defined as the location of the top of the centrifugal barrier, and is therefore a function of L. The strength of fragment attraction is treated as an adjustable parameter, which in turn affects the value of r_0. While $b_{\rm max}$ and r_0 are not the same, at each $E_{\rm avl}$ the value of r_0, averaged over L, roughly corresponds to $b_{\rm max}$. As shown in Fig. 4(a), for $C_6=4\times10^{-78}\,{\rm J\,m}^6$ and $L=8$–15 the maximum of $V_{\rm eff}$ is located at $r_0=3$–4 Å, while for $L<4$ it shifts to $r_0=6$–12 Å. This is comparable to the change in $b_{\rm max}$ with $E_{\rm avl}$ (4–7 Å), if we recognize that low L-values contribute near the dissociation threshold, while higher L-values are necessary to compensate for high $J_{\rm NCO}$ at higher excess energies. This interpretation is in accord with the barrierless nature of channel II dissociation.

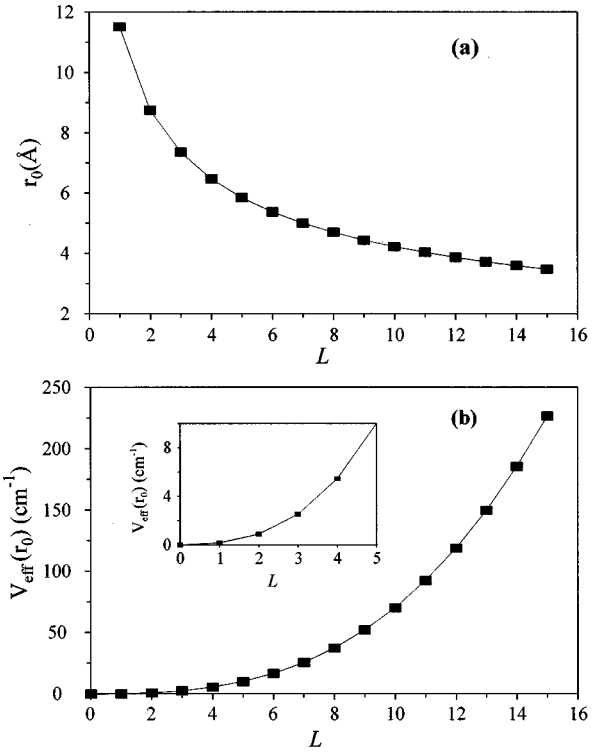

FIG. 4. Calculated (a) locations and (b) heights of the centrifugal barrier as a function of the orbital momentum quantum number, L, for the effective potential given by Eq. (4) with $C_6=4\times10^{-78}\,{\rm J\,m}^6$.

In Fig. 4(b), we also show the calculated centrifugal barrier heights as a function of L. Notice that even for small L, the barrier height is several wave numbers (see inset), and since $L\approx J$ ($J\equiv J_{\rm NCO}$), $V_{\rm eff}(r_0)$ soon exceeds the fragment c.m. translational energy, $E_t=E_{\rm avl}-E_J$ [where $E_J=BJ(J+1)$ is the rotational energy of NCO(J)]. Thus for HNCO the outer (rotational) TS may play a significant role even at relatively high available energies. This is in contrast to the unimolecular reactions of other polyatomic molecules (e.g., NCNO, CH_2CO, and NO_2) for which the reduced mass is larger, and both calculations and experiments indicate that except very near the threshold an inner (vibrational) TS determines the reaction rate.[1–5,8,31] Note, however, that due to inter-fragment exit-channel interactions, product rotational distributions are always more sensitive to the *outer* TS located near the top of the centrifugal barrier. For example, product rotational distributions often do not differ significantly from the predictions of *unconstrained* PST, even when the rates indicate that the TS has tightened.[5,8,32] As stated above, in the case of H+NCO the small reduced mass

and small NCO rotational constant lead to significant centrifugal barriers even at low excess energies.

2. Average rotational excitation in constrained PST

Additional insight into constrained PST can be obtained by considering approximate analytical expressions for the highest populated product rotational level, J_{max}, and the fraction of E_{avl} channeled into product rotation, $f_{rot}=\langle E_{rot}\rangle/E_{avl}$. In what follows, we consider the general case of decomposition into an atom and a linear fragment and apply the results to HNCO→H+NCO. We assume that: (i) the parent angular momentum is $J_0\approx 0$, and therefore Eq. (5) dictates $J\approx L$, where J is the rotational quantum number of the linear fragment, and (ii) $J_{max}\gg 1$, i.e., E_{avl} is not too small. From Eq. (3), we obtain,

$$\hbar^2 L_{max}^2\approx\mu^2\nu^2 b_{max}^2\approx\hbar^2 J_{max}^2. \tag{6}$$

Substituting

$$\nu^2=\frac{2E_t}{\mu}=\frac{2}{\mu}[E_{avl}-BJ(J+1)], \tag{7}$$

with $J=J_{max}\gg 1$ into Eq. (6) gives:

$$J_{max}^2\approx\frac{ab_{max}^2E_{avl}}{B(1+ab_{max}^2)}, \tag{8}$$

where

$$a=2B\mu/\hbar^2. \tag{9}$$

For H+NCO, $a=2.35\times10^{-2}$ Å^{-2}, and the unconstrained value $J_{max}\approx(E_{avl}/B)^{1/2}$ is reached only for $b_{max}>20$ Å. In contrast, when $b_{max}=4$ Å (e.g., for $E_{avl}=411\,cm^{-1}$), Eq. (8) gives $J_{max}\approx 0.5(E_{avl}/B)^{1/2}=17.5$, in good agreement with the experimental distribution shown in Fig. 3(a). Thus for $E_{avl}\approx 400\,cm^{-1}$, only half of the energetically allowed NCO rotational states are populated, indicating a severely constrained distribution even at the large impact parameters typical of a loose TS.

We now derive the dependence of f_{rot} on b_{max}. In unconstrained PST (i.e., in the limit of $b_{max}\to\infty$), the probability of producing a linear product in rotational state J, $P(J)$, is constant up to the energetic limit J_{max} (for a given NCO vibrational level), irrespective of E_{avl}. Therefore, the average product rotational energy (in the limit $J_{max}\gg 1$) is:

$$\langle E_{rot}\rangle=\frac{1}{J_{max}+1/2}\sum_{J=1/2}^{J_{max}}BJ(J+1)$$

$$\approx\frac{1}{J_{max}}\int_0^{J_{max}}BJ(J+1)dJ\approx\frac{1}{3}BJ_{max}^2 \tag{10}$$

(for a fragment whose lowest J quantum number is 1/2). For unconstrained PST, $BJ_{max}^2\approx E_{avl}$, and we obtain $f_{rot}=1/3$, as expected when the motions during dissociation are constrained to a plane.[33]

For constrained PST, J_{max} is expressed in terms of E_{avl} and b_{max}, as given by Eq. (8). If we assume that $P(J)$ is still constant (that is, the constraint affects only the value of J_{max}, whereas the shape of the distribution remains unaffected), then $\langle E_{rot}\rangle$ is still given by Eq. (10), and together with Eq. (8), we obtain:

$$f_{rot}=\frac{\langle E_{rot}\rangle}{E_{avl}}=\frac{ab_{max}^2}{3(1+ab_{max}^2)}. \tag{11}$$

For H+NCO, when $ab_{max}^2\gg 1$ (i.e., $b_{max}\gg 6.5$ Å), $f_{rot}\approx 1/3$ (the unconstrained value), while for $b_{max}=4$ Å, $f_{rot}=0.09$—a substantially lower fraction.

A more accurate value for f_{rot} can be obtained by explicitly using constrained PST to calculate $\langle E_{rot}\rangle$ without assuming a flat $P(J)$ distribution; the results for $E_{avl}=400\,cm^{-1}$ are shown in Fig. 5. In these calculations, the spin-orbit splitting in NCO was suppressed and two cases were considered: $T_{rot}(HNCO)=10$ K (with J_{HNCO} up to 6–7 substantially populated) and $J_{HNCO}=0$. Both calculations gave similar results, as well as the corresponding calculations for $E_{avl}=100\,cm^{-1}$. Again, f_{rot} is decreased from a limiting value of ~1/3 for $b_{max}>20$ Å to ~0.1 for $b_{max}=4$ Å, in good agreement with Eq. (11).

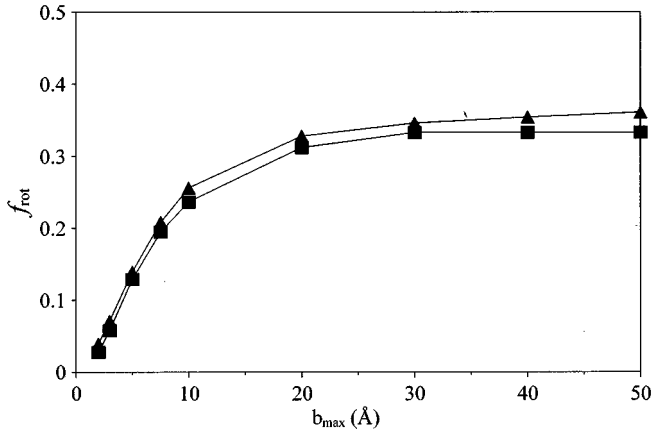

FIG. 5. The fraction of available energy channeled into NCO rotation, $f_{rot}=\langle E_{rot}\rangle/E_{avl}$, calculated by PST as a function of the limiting impact parameter, b_{max}. The calculations were carried out for $E_{avl}=400\,cm^{-1}$ assuming $J_{HNCO}=0$ (squares) and $T_{rot}=10$ K (triangles). Note the fast decrease in f_{rot} at $b_{max}<20$ Å. The spin-orbit multiplets of NCO are suppressed in these calculations.

B. The intramolecular decay of HNCO

1. Decay pathways near the H+NCO threshold

Although the $S_1(^1A'')\leftarrow S_0(^1A')$ spectrum of HNCO has not been fully assigned and its band origin is still unknown,[34] preliminary analysis indicates that most of the observed spectral features belong to ν_5' progressions; i.e., the NCO bending vibration is the most Franck–Condon active mode.[28,34–36] At low excitation energies, the spectrum appears regular, exhibiting *C*-type bands with well-resolved rotational structure.[28,29,34] However, some of the bands are broadened in all their rotational states, while others exhibit what appears to be state-specific perturbations.[14,29]

Channel I is open at all the excitation wavelengths studied, and the pathway to its formation, at least up to the channel III threshold, has recently been identified as $S_1\to S_0\to T_1\to{}^3$NH+CO.[20] As seen in Fig. 1, the ^{3}NH yield spec-

trum is very similar to the two-photon LIF excitation spectrum of HNCO.[14] In addition, no $S_1 \rightarrow S_0$ fluorescence is observed. The $S_1 \rightarrow S_0$ coupling matrix elements for IC can be estimated from the linewidths observed in the ^{3}NH yield or HNCO LIF excitation spectra. Assuming strong coupling for IC compared to the subsequent decay processes (see below), the spectral linewidths reflect mainly the $S_1 \rightarrow S_0$ decay rates. For bands with well-resolved structure, i.e., most of the bands excited at photolysis energies well below D_0(H+NCO), the homogeneous widths are $<0.8\,\mathrm{cm}^{-1}$, corresponding to lifetimes >6 ps, or coupling matrix elements $<0.01\,\mathrm{cm}^{-1}$ (using S_0 vibronic density of states of $\sim 1000/\mathrm{cm}^{-1}$ at $38\,000\,\mathrm{cm}^{-1}$).[37]

Near D_0(H+NCO), most bands no longer exhibit a well-resolved rotational structure,[14] indicating that the S_1 lifetime in this region is <6 ps. State-specific effects are still manifest in the linewidths of the vibronic bands,[14] apparently reflecting the existence of promoting modes on S_1 (although some influence of the accessed dark levels cannot be ruled out). Near the channel II threshold, IVR on S_0 should be complete, and IC should be essentially irreversible.

On S_0, we use a rate description to treat the competition between ISC and the decomposition to H+NCO, and assume that S_0 decay is decoupled from the preceding IC. The rate of channel I is controlled by the ISC rate, since only a modest barrier on T_1 ($\sim 1500\,\mathrm{cm}^{-1}$) exists in this channel,[38] and the region near D_0(H+NCO) is $>6000\,\mathrm{cm}^{-1}$ above this barrier. Thus on T_1 dissociation to channel I should be prompt. The branching ratio between channels I and II will depend on the ratios of their specific rates [given by Eqs. (1) and (2), respectively] at each photolysis energy.

2. Competition between dissociation to H+NCO and ^{3}NH+CO

Several observations related to the NCO and ^{3}NH photofragment yield spectra provide clues regarding the relative decay rates to channels I and II: (i) no abrupt decrease in the ^{3}NH yield is observed as the H+NCO channel opens; (ii) the increase in NCO($^2\Pi_{3/2}$) yield with E_{avl} scales roughly as the HNCO unimolecular decomposition rate (see below); (iii) even $\sim 5000\,\mathrm{cm}^{-1}$ above D_0(H+NCO), the ^{3}NH yield is significant, estimated at 10%–20% of the total dissociation yield.[20,29] Based on these observations, we argue that near the channel II threshold the ISC rate on S_0, $k_{\mathrm{ISC}}(E)$, must be several-fold faster than the rate of the unimolecular decay to H+NCO, $k_{\mathrm{uni}}(E)$.

The fractional yields of competing channels I and II, $Y_{\mathrm{I}}(E)$ and $Y_{\mathrm{II}}(E)$, can be expressed as

$$Y_{\mathrm{I}}(E) = k_{\mathrm{ISC}}(E)/[k_{\mathrm{ISC}}(E) + k_{\mathrm{uni}}(E)] \tag{12}$$

and

$$Y_{\mathrm{II}}(E) = k_{\mathrm{uni}}(E)/[k_{\mathrm{ISC}}(E) + k_{\mathrm{uni}}(E)]. \tag{13}$$

If the unimolecular decay of HNCO(S_0) were faster than ISC [i.e., $k_{\mathrm{uni}}(E) \gg k_{\mathrm{ISC}}(E)$], the yield of channel I would decrease markedly just above D_0(H+NCO)—contrary to the observations. In the opposite case [$k_{\mathrm{uni}}(E) \ll k_{\mathrm{ISC}}(E)$], the NCO yield [Eq. (13)] should increase with energy proportionally to $k_{\mathrm{uni}}(E)$, while the yield of channel I [Eq. (12)] near D_0(H+NCO) will be largely unaffected by the opening of channel II.

In the experiment, the ^{3}NH signal [Fig. 1(b)] does not decrease rapidly above the channel II threshold, as compared to the two-photon LIF spectrum of parent HNCO [Fig. 1(c)]. The ^{3}NH rotational distributions do not vary significantly with excitation energy over the energy range of Fig. 1, and therefore the relative peak heights in the ^{3}NH yield spectrum [Fig. 1(b)] reflect the total yield of channel I.

The NCO photofragment yield spectrum [Fig. 1(a)] was obtained by monitoring only the Q_{11}-bandhead of the $00^00\text{-}00^10$ transition, and it is not straightforward to convert the spectral intensities to total NCO yields. Even though the Q_{11}-branch is congested, its bandhead constitutes only a fraction of the total intensity of the NCO LIF spectrum. This fraction decreases considerably with excitation energy as a result of the fast rise in NCO average rotational excitation with increasing E_{avl} (Fig. 3). In addition, the second spin-orbit state of NCO (the $^2\Pi_{1/2}$ state) opens up at $E_{\mathrm{avl}} = 95\,\mathrm{cm}^{-1}$, and its yield increases with E_{avl}. Consequently, had $Y_{\mathrm{II}}(E)$ been constant, the observed peak heights in Fig. 1(a) should have *decreased* substantially with increasing E_{avl} compared to those in Figs. 1(b) and 1(c), which is obviously not the case. This is a qualitative indication that $Y_{\mathrm{II}}(E)$ *increases* with energy, as anticipated when $k_{\mathrm{ISC}}(E) > k_{\mathrm{uni}}(E)$.

We estimated $Y_{\mathrm{II}}(E)$ using the following procedure. First, from the simulated NCO fragment LIF spectra at the excitation energies indicated by arrows in Fig. 1(a), we determined the ratio of the Q_{11} bandhead intensity (integrated over the $0.2\,\mathrm{cm}^{-1}$ bandwidth) to the total integrated LIF spectrum. This ratio defined a spectral calibration factor *S*. We then normalized the measured NCO peak heights at each E_{avl} to the corresponding absorption peak heights (determined as the average of the ^{3}NH yield and the two-photon HNCO LIF peaks in spectra such as those in Fig. 1). Each normalized experimental peak height was then divided by the corresponding *S* value to give the estimated relative yield of NCO($^2\Pi_{3/2}$). Using this procedure, we estimate that the NCO yield in the region $E_{\mathrm{avl}} = 50\text{–}100\,\mathrm{cm}^{-1}$ is a factor of 2–3 smaller than in the 350–400 cm^{-1} range. In the limit $k_{\mathrm{uni}}(E) \ll k_{\mathrm{ISC}}(E)$, this increase in $Y_{\mathrm{II}}(E)$ with excitation energy reflects the increase in the rate of the unimolecular decomposition to H+NCO($^2\Pi_{3/2}$).

We estimated the H+NCO($^2\Pi$) unimolecular decomposition rate, $k_{\mathrm{uni}}(E)$, using the same constrained PST model that fits the rotational distributions, i.e.,

$$k_{\mathrm{uni}}(E) = g_{\mathrm{NCO}} \sum_{s-o} \sum_{J_{\mathrm{NCO}}} \frac{g_L(J_{\mathrm{NCO}})}{h\rho(E)} = \frac{N^{\dagger}(E)}{h\rho(E)}, \tag{14}$$

where $g_{\mathrm{NCO}} = 2$ is the electronic degeneracy of NCO($^2\Pi$), $g_L(J_{\mathrm{NCO}})$ is the number of allowed *L* states per J_{NCO} state, $\rho(E)$ is the total density of states of HNCO, and the summations are over J_{NCO} and the two spin-orbit states of NCO. Since over a narrow energy range, $k_{\mathrm{uni}}(E)$ increases approximately as $N^{\dagger}(E)$, we display in Fig. 6 the variation of $N^{\dagger}(E)$ with E_{avl} for $J_{\mathrm{HNCO}} = 2$. In this calculation, we assumed a statistical population of the two spin-orbit states of NCO.

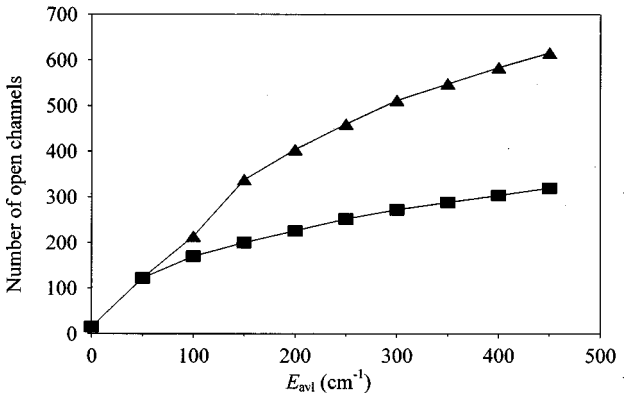

FIG. 6. The number of open channels calculated by PST for HNCO→H+NCO decomposition as a function of E_{avl}. The triangles indicate the total number of open channels to the two spin-orbit states of NCO($^2\Pi_{1/2,3/2}$), while the squares show the corresponding number leading to the formation of the lowest spin-orbit state, $^2\Pi_{3/2}$. In the calculations, $J_{HNCO}=2$ and $C_6=4\times10^{-78}$ J m^6 are used. The calculated points are connected by lines for convenience of viewing.

Also shown in Fig. 6 are the $N^\dagger(E)$ values corresponding solely to the H+NCO($^2\Pi_{3/2}$) channel. It is this curve that should be compared with the relative NCO yields derived from the experimental results. We find that $N^\dagger(E)$ increases by a factor of 2.7 between $E_{avl}=50$ and 400 cm^{-1}, which is in reasonable accord with the increase in NCO yield estimated from the experimental data. Thus all the data are consistent with the interpretation that at least up to $E_{avl}=400$ cm^{-1}, $k_{ISC}(E)$ exceeds $k_{uni}(E)$ be a factor of at least 5.[39]

The calculation of $k_{uni}(E)$ [Eq. (14)) assumes that the rate is determined at the outer (rotational) TS, located at the top of the centrifugal barrier. However, as discussed above, an inner (vibrational) TS determined variationally becomes important with increasing excitation energy, which may further reduce $k_{uni}(E)$.[1,2] Without detailed calculations, it is hard to predict at what excess energy the inner TS becomes important. Thus $k_{uni}(E)$ calculated by Eq. (14) should be considered as an upper limit.

The absolute values of $k_{uni}(E)$ calculated by Eq. (14) are approximate also because of the uncertainty in $\rho(E)$. In PST, $\rho(E)$ is given by the density of vibrational states (ρ_V) and rotational K-levels of a prolate top (ρ_K).[1,2,6,7] If we assume that K is not conserved in the dissociation, then $\rho(E)=\rho_{V,K}\approx(2J_0+1)\rho_V$, whereas for conserved K, $\rho(E)=\rho_V$. Assuming that K is not conserved and $\rho_V=1000/\text{cm}^{-1}$,[37] the upper limits to k_{uni} for $E_{avl}=50-400$ cm^{-1} are in the range $(0.7-3.7)\times10^9$ s^{-1}. The $S_0\rightarrow T_1$ ISC rates should then be of the order of 10^{10} s^{-1} or faster. If K is conserved, the above rates should be multiplied by $(2J_0+1)$. In order to determine $k_{uni}(E)$ experimentally, the branching ratios to channels I and II need to be known, as well as the total S_0 decay rate. The latter can be determined from time-resolved measurements of the appearance of ^{3}NH or NCO.

V. SUMMARY

Near its threshold, the H+NCO channel in HNCO decomposition evolves on the ground-state PES without a barrier. The NCO rotational distributions at $E_{avl}=17-411$ cm^{-1} are well described by PST, provided that dynamical constraints are included. These constraints can be expressed either by a b_{max} fit parameter, or as arising from centrifugal barriers that determine the location of the outer TS. Both approaches reflect the same physical reality by eliminating unphysical parts of fragment phase space. We find that even for a loose TS located at 4–7 Å, the fraction of E_{avl} deposited as fragment rotational energy is much smaller than the fraction predicted by unrestricted PST. The reduction is typical of systems of small reduced mass, and can be approximately described as a function of impact parameter with a simple analytical formula.

In using the centrifugal-barrier constraint, it is possible to fit all the rotational distributions by describing the long-range attractive interfragment interaction with an LJ potential. The use of this model involves approximations regarding the potential anisotropy. Our analysis shows that orientation averaging of the potential results in a shift of the effective origin of the fragment interaction with respect to the center of mass of the polyatomic fragment, and attenuation of the magnitude of the potential.

We have also discussed the competition on HNCO(S_0) between unimolecular decomposition to H+NCO and ISC followed by dissociation to ^{3}NH+CO, and concluded that near the H+NCO channel threshold ISC must be several-fold faster.

ACKNOWLEDGMENTS

We wish to thank P. J. Dagdigian for providing the spectral analysis programs for NCO LIF, K. Morokuma for communicating results prior to publication, and S. Klippenstein for helpful discussions. Support by the National Science Foundation is gratefully acknowledged.

APPENDIX. ORIENTATION-AVERAGING OF THE LONG-RANGE POTENTIAL IN PLANAR ATOM-MOLECULE DISSOCIATION: APPLICATION TO H+NCO

The determination of the height and position of the centrifugal barrier in unimolecular decomposition requires knowledge of the fragment interaction potential. For polyatomic molecules, the center of interfragment interaction does not usually coincide with the fragment's center of mass, since bonds are directional, and the potential depends on the relative orientation of the fragments. Therefore, the effective potential in Eq. (4) cannot be defined as a function of a single coordinate R or r. However, for a loose TS with free fragment internal rotation, the anisotropic potential can be orientation averaged, reducing the problem to a one-dimensional case, as in diatomic dissociation.

In what follows, we consider the specific case of HNCO→H+NCO, but a generalization to other systems is straightforward. We assume that the interaction of the separating H and NCO fragments can be described in terms of

only the N–H attraction, and the potential scales as r^{-6} (LJ potential). We show that the orientation-averaged potential can be written in terms of the center-of-mass coordinate R as an LJ potential *shifted to larger fragment separations.* On average, the moving center of attraction (N) appears to the H fragment as a circle of effective radius $a=0.9$ Å, centered at the NCO center of mass. The isotropic (averaged) potential still scales as an LJ potential, but with the distance measured from H to the effective circle.

The following assumptions are made: (i) at separations characteristic of a loose TS, the H fragment interacts attractively only with the N atom; (ii) the interaction potential is given by

$$V(r)=-\frac{C_6}{r^6}, \tag{A1}$$

where r is the N–H distance; (iii) HNCO is planar and all the forces during dissociation act in the plane; and (iv) dissociation can be modeled by PST, i.e., the dissociation trajectories sample a significant portion of the planar H–NCO potential.

With R defined as the distance from H to the NCO center of mass (X), let r_N be the X–N distance ($r_N=1.2$ Å), while θ is the HXN angle. The H–NCO potential defined by Eq. (A1) is anisotropic with respect to the NCO center of mass, and can be expressed in terms of R and θ:

$$V(R,\theta)=-\frac{C_6}{(R^2+r_N^2-2R\cdot r_N\cdot\cos\theta)^3}. \tag{A2}$$

The effective attraction experienced by the fragments as a function of R is the angular average of the potential in Eq. (A2). For planar dissociation,

$$V(R)=\langle V(R,\theta)\rangle_\theta$$

$$=-\frac{C_6}{2\pi}\int_0^{2\pi}\frac{d\theta}{(R^2+r_N^2-2R\cdot r_N\cdot\cos\theta)^3}. \tag{A3}$$

While this integral can be solved analytically, the solution is cumbersome, and instead we use a numerical solution for the specific case of H+NCO. The solution is shown by solid circles in Fig. A1(a), which give the average potential $V(R)/C_6$ as a function of R. The functional dependence in Eq. (A3) is different than that given by the familiar LJ-type potential

$$V^*(R)=-\frac{C_6^*}{R^6}. \tag{A4}$$

As shown in Fig. A1(a), no single curve of the functional form given by Eq. (A4) results in a satisfactory fit over the entire range of R. The approximate potential $V^*(R)$ that is in good agreement with the exact potential $V(R)$ for $R>4$ Å corresponds to $C_6^*/C_6=2.0$, while the fit reproducing better the short-range behavior corresponds to $C_6^*/C_6=3.2$. The failure to describe correctly the entire potential range results from the inadequacy of replacing the $1/r^6$ term in Eq. (A1) by $1/R^6$. Because of the power dependence, the effect of displacement of the potential origin from the NCO center of mass to N cannot be averaged out by NCO rotation ($\langle 1/r^6\rangle \neq 1/\langle r\rangle^6$).

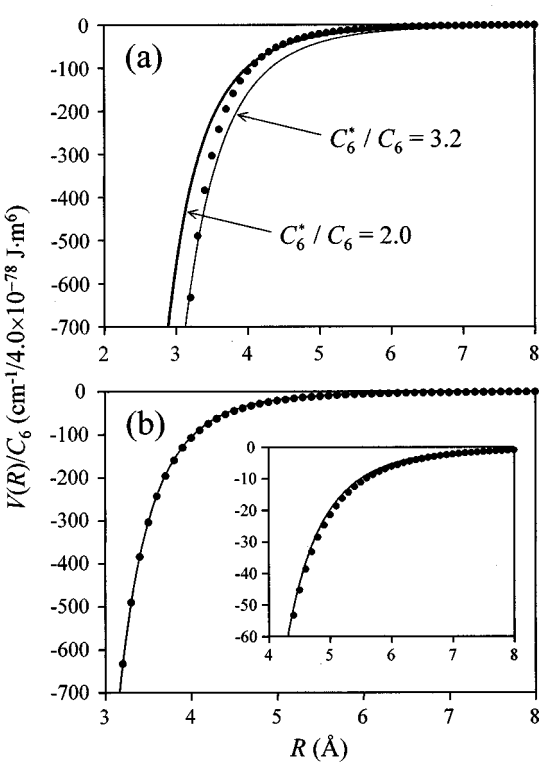

FIG. A1. (a) Solid circles: average potential $V(R)$ defined by Eq. (A3), with $r_N=1.2$ Å, normalized to an arbitrary chosen value of $C_6=4.0\times10^{-78}$ J m^6. Thick curve and hairline: fits using the approximate potential $V^*(R)$ in Eq. (A4) with $C_6^*/C_6=2.0$ and 3.2, respectively. (b) Solid circles: average potential $V(R)$ [Eq. (A3) with $r_N=1.2$ Å], normalized to $C_6=4.0\times10^{-78}$ J m^6 [reproduced from (a)]. Solid line: a least-squares fit using an approximate potential $V^{**}(R)$ defined by Eq. (A5), yielding $C_6^{**}/C_6=0.47$ and $a=0.90$ Å. The inset expands the long-range part of the graph for convenience of comparison. In both (a) and (b), the vertical axis has the same units.

A much better approximation of $V(R)$ in Eq. (A3) is given by

$$V^{**}(R)=-\frac{C_6^{**}}{(R-a)^6}. \tag{A5}$$

A least-squares fit of Eq. (A5) to the solution of Eq. (A3) is shown in Fig. A1(b) by the solid line. This fit is obtained with $C_6^{**}/C_6=0.47$ and $a=0.90$ Å. The good quality of the fit over the entire range supports the use of Eq. (A5), to which we offer a simple interpretation. When NCO rotates about its center of mass, the N atom appears to the H fragment, on average, as a circle of effective radius $a(a\neq r_N)$ centered at the NCO center of mass. The potential scales as $1/r^6$, where r is now the distance from the effective circle: $r=R-a$.

Mathematically, the potential shift reflects the fact that $\langle 1/r^6\rangle > 1/\langle r\rangle^6$, which makes the average LJ attractive force appear closer in origin to the H fragment than dictated by the average H–N distance ($\langle r\rangle=R$). In other words, due to the negative-power dependence of the potential, those parts of the N orbit that are closer to H contribute more to the average attraction than remote points. At the same time, the average effective potential magnitude is attenuated (C_6^{**}/C_6

$=0.47$), since the attraction center N spends only a fraction of time in those parts of its orbit that contribute the most to the potential.

In general, any anisotropic potential expressed as a polynomial expansion $V(r)=-\Sigma C_n r^{-n}$ ($n>0$) can be averaged following the treatment suggested here to yield

$$V^{**}(R)=-\sum_n \frac{C_n^{**}}{(R-a_n)^n}, \tag{A6}$$

where the C_n^{**} and a_n coefficients have similar meanings as in Eq. (A5).

While these considerations are general, we are nevertheless able to reproduce all the experimental results using Eq. (A4) with $C_6^*=(4\pm2)\times10^{-78}\,\mathrm{J\,m^6}$. This is not surprising considering the looseness of the TS for a typical barrierless dissociation. Notice that at large fragment separations there is good agreement between Eq. (A3) and the approximate form given by Eq. (A4) [Fig. A1(a)]. Since the long-range fit in Fig. A1(a) gives $C_6^*/C_6=2.0$, we expect the true value of C_6 for the H–N interaction in HNCO to be smaller than the value obtained by using Eq. (4) in the main text; i.e., $C_6\approx(2\pm1)\times10^{-78}\,\mathrm{J\,m^6}$.

In summary, orientation averaging of any anisotropic negative-power-law potential $V(r)$ (where r is the dissociated bond length) yields a one-dimensional potential $V(R)$ (where R is the fragment c.m. separation) that can be approximated by the same functional form as the original potential. However, it is attenuated in magnitude and its effective origin is shifted with respect to the center of mass of the polyatomic fragment.

[1] R. G. Gilbert and S. C. Smith, *Theory of Unimolecular and Recombination Reactions* (Blackwell, Oxford, 1990).
[2] T. Baer and W. L. Hase, *Unimolecular Reaction Dynamics* (Oxford University Press, Oxford, 1996).
[3] W. H. Green, Jr., C. B. Moore, and W. F. Polik, Annu. Rev. Phys. Chem. **43**, 591 (1992), and references therein.
[4] S. A. Reid and H. Reisler, Annu. Rev. Phys. Chem. **47**, 495 (1996); J. Phys. Chem. **100**, 474 (1996), and references therein.
[5] H. Reisler and C. Wittig, Annu. Rev. Phys. Chem. **37**, 307 (1986); *Advances in Chemical Kinetics and Dynamics*, edited by John R. Barker (JAI Press, Greenwich, 1992), p. 139.
[6] See papers and discussion in Faraday Discuss. Chem. Soc. **102** (1995).
[7] H. F. Davis, K. Mikhaylichenko, L. Valachovic, S. Ionov, R. A. Beaudet and C. Wittig, J. Chem. Phys. **101**, 4809 (1994); P. Ionov, I. Bezel, and C. Wittig, Chem. Phys. Lett. **272**, 257 (1997).
[8] C. B. Moore and I. W. M. Smith, J. Phys. Chem. **100**, 12848 (1996); A. Mellinger, M. V. Ashikhmin, and C. B. Moore, J. Chem. Phys. **108**, 8944 (1998).
[9] C. X. W. Qian, A. Ogai, H. Reisler, and C. Wittig, J. Chem. Phys. **90**, 209 (1989).
[10] C. G. Morgan, M. Drabbels, and A. M. Wodtke, J. Chem. Phys. **105**, 4550 (1996); C. G. Morgan and A. M. Wodtke, Adv. Photochem. **23**, 27 (1997).
[11] W. K. Yi and R. Bersohn, Chem. Phys. Lett. **206**, 365 (1993).
[12] B. Ruscic and J. Berkowitz, J. Chem. Phys. **100**, 4498 (1994).
[13] J. Zhang, M. Dulligan, and C. Wittig, J. Phys. Chem. **99**, 7446 (1995).
[14] (a) M. Zyrianov, A. Sanov, Th. Droz-Georget, and H. Reisler, Roy. Soc. Chem. Faraday Disc. **102**, 263 (1995); (b) M. Zyrianov, Th. Droz-Georget, A. Sanov, and H. Reisler, J. Chem. Phys. **105**, 8111 (1996).
[15] S. S. Brown, H. L. Berghout, and F. F. Crim, J. Chem. Phys. **105**, 8103 (1996); *ibid.* **102**, 8440 (1995); *ibid.* **107**, 8985 (1997); *ibid.* **106**, 5805 (1997); S. S. Brown, R. B. Metz, H. L. Berghout, and F. F. Crim, J. Phys. Chem. **100**, 7948 (1996).
[16] (a) R. A. Brownsword, T. Laurent, R. K. Vatsa, H.-R. Volpp, and J. Wolfrum, Chem. Phys. Lett. **249**, 162 (1996); (b) *ibid.* **258**, 164 (1996); (c) R. A. Brownsword, M. Hillenkamp, T. Laurent, R. K. Vatsa, and H.-R. Volpp, J. Chem. Phys. **106**, 4436 (1997).
[17] T. A. Spiglanin, R. A. Perry, and D. W. Chandler, J. Phys. Chem. **90**, 6184 (1986).
[18] S. S. Brown, R. B. Metz, H. L. Berghout, and F. F. Crim, J. Phys. Chem. **105**, 6293 (1996); H. L. Berghout, S. S. Brown, R. Delgado, and F. F. Crim, *ibid.* **109**, 2257 (1998).
[19] Th. Droz-Georget, M. Zyrianov, A. Sanov, and H. Reisler, Ber. Bunsenges. Phys. Chem. **101**, 469 (1997).
[20] M. Zyrianov, Th. Droz-Georget, and H. Reisler, J. Chem. Phys. **110**, 2059 (1999).
[21] J. E. Stevens, Q. Cui, and K. Morokuma, J. Chem. Phys. **108**, 1452 (1998).
[22] J. Klossika, H. Floethmann, C. Beck, R. Schinke, and K. Yamashita, Chem. Phys. Lett. **276**, 325 (1997).
[23] (a) P. Pechukas, J. C. Light, and C. Rankin, J. Chem. Phys. **44**, 794 (1966); (b) P. Pechukas and J. C. Light, *ibid.* **42**, 3281 (1965); (c) J. C. Light, Discuss. Faraday Soc. **44**, 14 (1967).
[24] C. X. W. Qian, M. Noble, I. Nadler, H. Reisler, and C. Wittig, J. Chem. Phys. **83**, 5573 (1985).
[25] P. J. Dagdigian, private communication; D. G. Sauder, D. Patel-Misra, and P. J. Dagdigian, J. Chem. Phys. **95**, 1696 (1991); S. A. Wright and P. J. Dagdigian, *ibid.* **104**, 8279 (1996), and references therein.
[26] A. Ogai, C. X. W. Qian, and H. Reisler, J. Chem. Phys. **93**, 1107 (1990).
[27] R. A. Ashby and R. L. Werner, J. Mol. Spectrosc. **118**, 184 (1986).
[28] M. Zyrianov, Ph. D. thesis, University of Southern California (1998).
[29] M. Zyrianov, Th. Droz-Georget, and H. Reisler, J. Chem. Phys. **106**, 7454 (1997).
[30] A. C. Terentis, S. E. Waugh, G. F. Metha, and S. H. Kable, J. Chem. Phys. **108**, 3187 (1998).
[31] S. J. Klippenstein, A. L. L. East, and W. D. Allen, J. Chem. Phys. **101**, 9198 (1994); *ibid.* **105**, 118 (1996); S. J. Klippenstein, *ibid.* **101**, 1996 (1994).
[32] S. A. Reid, D. C. Robie, and H. Reisler, J. Chem. Phys. **100**, 4256 (1994).
[33] In the classical limit, $f_{\mathrm{rot}}=1/3$ can be obtained from the basic statistical postulates simply by recognizing that in planar dissociation (in the absence of vibrational excitation), there are three active degrees of freedom: two translational and one rotational.
[34] R. N. Dixon and G. H. Kirby, Trans. Faraday Soc. **64**, 2002 (1968) .
[35] F. F. Crim (private communication).
[36] M. Zyrianov and H. Reisler (unpublished).
[37] The harmonic count of vibrational states near $D_0(\mathrm{H+NCO})$ gives $\rho\sim400/\mathrm{cm^{-1}}$; however, this number does not take into account the existence of structural isomers of HNCO (e.g., HCNO, HOCN) whose densities of states are unknown, nor does it include anharmonic corrections, which are likely to substantially increase the density of states of $\mathrm{HNCO}(S_0)$.
[38] A. M. Mebel, A. Luna, M. C. Lin, and K. Morokuma, J. Chem. Phys. **105**, 6439 (1996).
[39] When the ratio is smaller, deviations from the behavior predicted by Eq. (14) are observed.